ACS APPLIED MATERIALS & INTERFACES

Letter

www.acsami.org

Synthesis and Optoelectronic Properties of Two-Dimensional FeS_2 Nanoplates

Alec Kirkeminde,[†] Brian A. Ruzicka,[‡] Rui Wang,[‡] Sarah Puna,[†] Hui Zhao,[‡] and Shenqiang Ren*[,†]

[†]Department of Chemistry, [‡]Department of Physics and Astronomy, University of Kansas, Lawrence, KS, USA 66045.

Supporting Information

ABSTRACT: There is a growing interest in the earth abundant and nontoxic iron disulfide (FeS_2) photovoltaic materials. Here, we report the synthesis of FeS_2 nanoplates with different spectral features which we have associated with thicknesses and crystallization. The structure and crystalline order of ultrathin FeS_2 nanoplates have a strong influence on the carrier lifetime, electronic and optical properties. We demonstrate that two-dimensional FeS_2 nanoplates show great promise for fabrication of hybrid bulk heterojunction solar cells. This opens up a host of applications of these materials as inexpensive solar cells and photocatalysts.

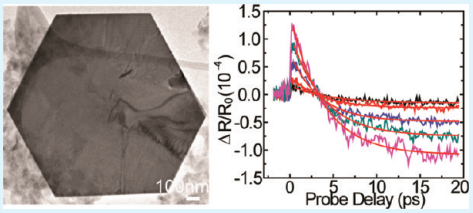

KEYWORDS: *colloidal synthesis, iron disulfide (FeS_2), nanoplates, carrier lifetime, hybrid solar cells*

1. INTRODUCTION

Iron disulfide (FeS_2), with a pyrite structure, has significant scientific interest and technological applications.[1−3] On the application side, FeS_2, is the major sulfur mineral in coal, and has demonstrated a significant increase in photoelectrochemical activities.[4] Owing to their large potential capacities for solar cell applications, iron-based materials have been extensively studied as possible alternatives for commercially available silicon or gallium arsenide solar cells.[5] Compared with other multi-composition photovoltaic materials such as Cu_2ZnSnS_4,[6,7] binary FeS_2 nanocrystals allow solution-processed solar cells. Recent efforts on research and development of pyrite FeS_2 nanocrystals have been driven by remarkable performance improvements of low cost solar cells to meet ever-increasing energy demands.[8] However, the main drawback of this system is stemming from oxidation and due to the orthorhombic metastable marcasite structure that is detrimental to photovoltaic properties.[9]

Though various FeS_2 spherical nanoparticles have been fabricated using a variety of synthetic methods,[10,11] thus far the preparation of high quality two-dimensional (2D) layered FeS_2 nanoplates has remained a significant challenge. The electronic structures of FeS_2 and other 3d transition metal dichalcogenides have been of considerable scientific interest because these materials straddle the localization-itinerant regimes for the 3d electrons.[12−14] It is important to understand how this structure varies with electronic confinement, but apparently no earlier work exists on this subject. Especially, in layered FeS_2 nanoplates, the lateral confinement can remarkably enhance optoelectronic performance compared to their bulk counterparts because of nanoscale characteristics that include large surface areas, finite lateral sizes, and enhanced open-edge morphologies.

In this letter, we report the development of a facile synthesis of laterally confined, 2D, and layered FeS_2 nanoplates. Because of its unique morphology, consisting of a finite lateral sized and well-defined layered structure, this material is more suitable for many applications in comparison to its nanoparticle counterparts. In fact, as a material with layered crystal structure, FeS_2 nanocrystals with sheet or plate shape may be more attractive due to the probable quantum confinement at one dimension and the electrical continuity at the other two dimensions. Below, we discuss the morphological and optical properties of this substance and its potential utilization as a photovoltaic material.

2. EXPERIMENTAL SECTION

Laterally confined 2D FeS_2 nanoplates were synthesized by using thermal decomposition of the precursor, $Fe(CO)_5$, in an organic solvent at elevated temperature. All of the synthetic experiments were carried out under Ar atmosphere using standard Schlenk line techniques. In a typical synthesis of FeS_2 nanoplates, the sulfur stock solution was prepared by the coordinating solvent oleyamine (OLA) with elemental sulfur and deaerated at different temperatures (120 °C, 180 and 240 °C, referred as the reaction temperature later) for 15 min and then backfilled with Ar for 15 min. In a separate vessel, $Fe(CO)_5$ organometallic precursor is dissolved and heated under Ar. At the reaction temperature, $Fe(CO)_5$ was rapidly injected into the sulfur solution, while not permitting the temperature of the solution to decrease. The vessel with the resulting black mixture was continually stirred at this temperature for different aging time (3, 30, 60, 180, and 540 min). After the mixture was cooled to room temperature, methanol was added to precipitate the product. The black precipitate was then isolated via the centrifugation (3000 rpm)

Received: January 17, 2012
Accepted: February 10, 2012
Published: February 10, 2012

   dx.doi.org/10.1021/am300089f | ACS Appl. Mater. Interfaces 2012, 4, 1174−1177

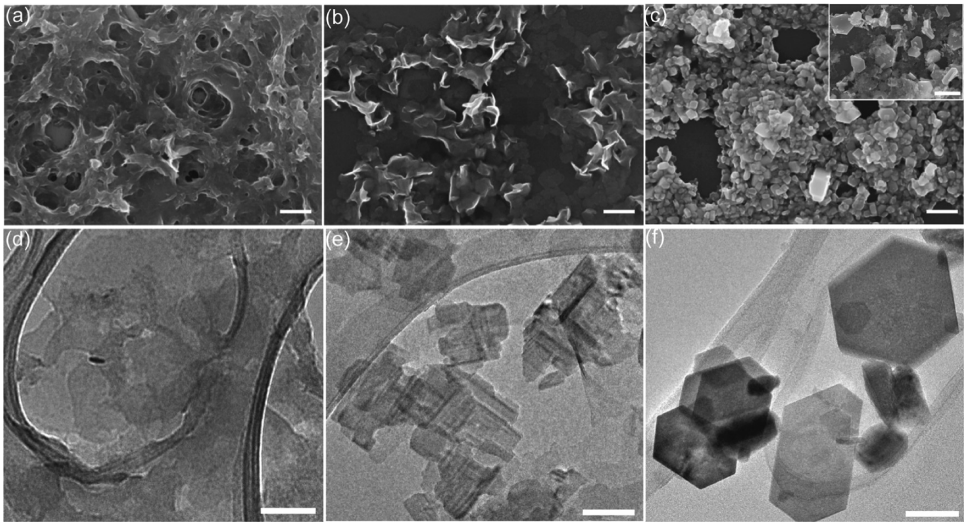

Figure 1. Scanning electron microscopy (SEM) and transmission electron microscopy (TEM) images of FeS_2 nanocrystals synthesized at (a) the reaction temperature and (d) 120 °C, (b, e) 180 °C and (c, f) 240 °C, respectively. The scale-bar is 200 nm.

for 5 min. The washing process was repeated three times with methanol to ensure removal of any excess capping agent. The final FeS_2 nanoplates were obtained by dissolving into chloroform.

3. RESULTS AND DISCUSSION

The structure of the crystalline platelike FeS_2 is strongly dependent on the reaction temperature and aging time. Field emission scanning electron microscopy (FESEM) and transmission electron microscopy (TEM) images show the FeS_2 morphologies with 180-min aging time at different reaction temperatures: 120 °C, 180 and 240 °C. At a low temperature of 120 °C, the reactants mostly form an amorphous precursor state without clear edges (Figure 1a,d). Irregular, continuous material is seen (Figure 1a), and no isolated particles can be found. This shows the presence of undecomposed precursor at this low temperature. Increasing the reaction temperature to 180 °C promotes the appearance of nanoplates with a clear edge. The FeS_2 nanocrystalline are 2D nanoplates with a lateral size of ca. 150 nm and size distribution of (20%) (Figure 1b and 1e). The FeS_2 samples prepared at 180 °C are mainly composed of nanoplates with irregular shapes. Upon increasing reaction temperature to 240 °C, the FeS_2 nanoplates have a truncated hexagonal and triangular shape with a large size variation from 200 to 500 nm, as shown in the SEM and TEM images (Figure 1c, f and Figure S1a in the Supporting Information). The increased reaction temperature plays an important role in the 2D planar growth but with a minor effect on the thickness of FeS_2 nanoplates, which is about 30 nm thickness. The anisotropic growth of the FeS_2 nanoplate may originate from the crystalline facets which tend to develop on the low-index planes to minimize the surface energy when growing.[15] The platelike FeS_2 nanocrystals with regular shape are formed exhibiting mainly hexagonally shaped nanoplates (Figure 1f). This further demonstrates that the reaction temperature plays a very important role in the formation of nanoplates. The chemical components of the nanoplates have been identified by energy dispersive X-ray spectroscopy (see Figure S1 in the Supporting Information).[16−18]

The FeS_2 nanoplate growth process can also be demonstrated by changing the aging time while keeping the same reaction temperature of 180 °C. We investigated the morphology and structure of FeS_2 nanoplates using TEM and high-resolution TEM. Figure 2 shows typical TEM images of

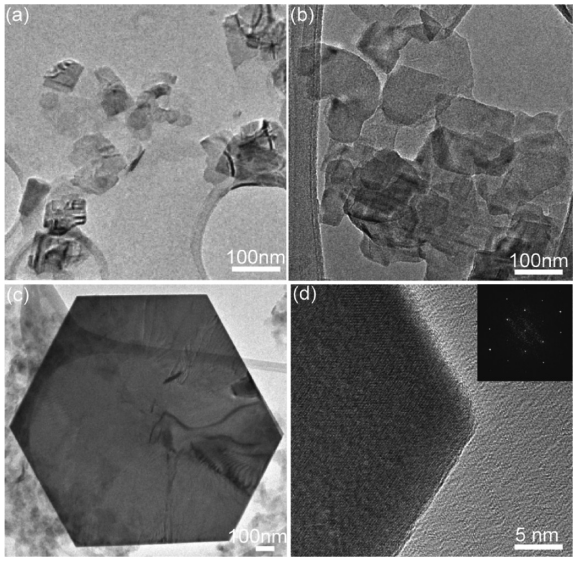

Figure 2. TEM images of FeS_2 nanoplates at 180 °C reaction temperature of different aging time: (a) 3, (b) 180, and (c) 240 min. (d) High-resolution TEM image of hexagonal lattice structure of FeS_2 nanoplates, with the inset image showing a selective area electron diffraction pattern.

the FeS_2 nanoplates with varied aging time. The particles show platelike shapes for the 3-min aging time (Figure 2a). The nanoplates had no uniform shape and size, demonstrating an incomplete reaction at this time. However, the crystal lattice fringes of this sample can still be observed, suggesting a fast crystallization at the beginning of reaction. At the same reaction temperature, the nanoplates start to grow larger and thicker with increasing aging time. Compared to the 3 min aging time, FeS_2 nanoplates aged for 180-min grow bigger and thicker but remain relatively thin (Figure 2b). After 540 min aging, nanoplates with regular shape and increased thickness can be obtained. A single hexagonal FeS_2 nanoplate with the HRTEM

dx.doi.org/10.1021/am300089f | ACS Appl. Mater. Interfaces 2012, 4, 1174−1177

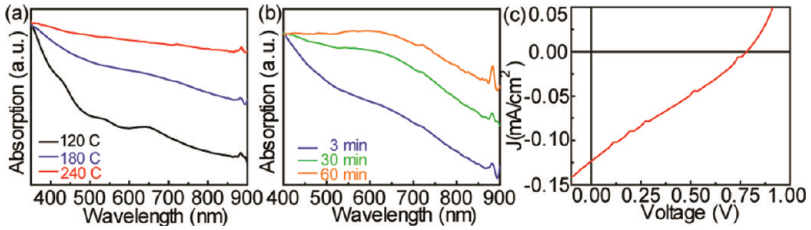

Figure 3. (a) Absorption spectra of FeS_2 nanoplates at 3 min aging time with different reaction temperature. (b) Absorption spectra of FeS_2 nanoplates at 180 °C reaction temperature with different aging time. (c) Current−voltage characteristics of FeS_2/P3HT hybrid solar cells under AM1.5 1-sun illumination.

image is shown in Figure 2c,d. The selective area of electron diffraction (SAED, inset Figure 2d) pattern was obtained by aligning the electron beam perpendicular to the face of this plate. The hexagonally symmetric spots pattern indicates the single crystallinity and can be indexed based on a cubic cell with a lattice parameter of 0.542 nm. The clear lattice fringes shown in Figure 2d indicate that the nanoplate is highly crystallized. The spacing of 0.938 nm corresponds to the (111) planes of FeS_2. Interestingly, although the planar dimension is more than 2 um, the plate is transparent under the electron beam, indicating that the plate is very thin. The shape variation from irregular thin platelike morphology to regular thick hexagonal nanoplates suggests an Ostwald growth mechanism. Mainly, at the beginning of growth time, crystalline seeds are readily combined in a random fashion to form very thin and irregular crystals. After a longer growth time, whereas FeS_2 nanoplates become thicker, more and more seeds participate in the action of assembling at the thicker edge of the nanoplate due to a smaller, more stable crystalline lattice energy compared to forming an irregular thick nanoplate. It should be noted that the variation of nanoplate shape results from the different growth speed along different crystal directions. Based on the discussed FeS_2 growth, we can see that nanoplate-shaped FeS_2 can be obtained through two different paths. One path of two-dimensional FeS_2 growth is through direct nanoplates growth from small size to larger ones at high reaction temperature, and the other one can happen at a relatively low reaction temperature but at longer aging time. Both of the two pathways enable the formation of well-defined, regular FeS_2 nanoplates.

The photoabsorption behavior of FeS_2 nanoplates is essential for their optoelectronic applications. The absorbance spectra of FeS_2 nanoplates are shown in Figure 3. Panels a and b in Figure 3 show the sequence of optical absorption spectra of FeS_2 nanoplates with varied reaction temperatures and aging time. In the Figure 3a, the apparent absorption versus photon energy under the same aging time of 180 min is plotted. As we can see, the first excitonic absorption peak at 895 nm (1.38 eV) corresponds to the direct bandgap of FeS_2.[19,20] The spectral curves vary with the reaction temperature showing a faster growth at about 180−240 °C, which gives rise to an upshift of the absorption spectra as the temperature is increased. Under the same reaction temperature of 180 °C, the photoabsorption can be enhanced by increasing the aging time. The feature identified as the first excitonic transition does not change, only the absorption in the whole photoactive spectrum. All other distinct features are direct transitions from deep in the valence band to the conduction band. Given the layered nature of the FeS_2 nanostructures, we have fabricated and tested the photovoltaic performance of organic P3HT and inorganic FeS_2 nanoplate hybrid solar cells. By blending the P3HT and FeS_2 at 1:1 volume ratio, a bulk heterojunction solar cell with a large open circuit voltage of 0.78 V and AM 1.5 power conversion efficiency of 0.03% is achieved (Figure 3c, see Supporting Information for details). Though the efficiency is low, this is the first time to demonstrate that environmentally friendly and low-cost FeS_2 nanoplates can be used as a promising electron acceptor in hybrid solar cells.

The low efficiency observed motivated us to investigate the charge carrier dynamics in this new material in order to explore potential improvements, because it is known that the photoexcited carrier lifetime, which controls the carrier density, is one of the major factors limiting the efficiency. We use an optical ultrafast pump−probe technique to measure carrier lifetime (see Figure S2 in the Supporting Information).[21] The sample is kept in a vacuum chamber to prevent oxidation during measurements. A pump laser pulse of 100 fs and 750 nm injects charge carriers by exciting electrons from the valence band to the conduction band. These carriers are probed by a time-delay probe pulse of 100 fs and 810 nm. Reflection of the probe is collected and sent to a photodiode, which output is measured by a lock-in amplifier. But modulating the intensity of the pump beam with a mechanical chopper, we can measure the differential reflection, defined as $\Delta R/R_o = (R - R_o)/R_o$, where R and R_o are the reflections with and without the presence of the pump, respectively. The transmitted probe is also collected and guided to the detector, in order to measure the differential transmission, defined similarly as $\Delta T/T_o = (T - T_o)/T_o$.

Figure 4a shows the measured differential transmission signal as a function of the probe delay (the arriving time of the probe pulse at the sample with respect to the pump pulse) with several energy fluencies of the pump pulse. The signal is negative initially, and changes to positive after several ps. A negative differential transmission means the absorption is increased by the pump, which could be induced by free-carrier absorption. The signal decays exponentially, with a time constant of 2.4 ± 0.5 ps. After the transient time of about 20 ps, a positive steady signal is detected. It is likely induced by the heating effect of the pump pulse. By comparing the results from different pump fluences, we found that the signal is proportional to the pump fluence, as shown in Figure 4c. Because the injected carrier density is proportional to the pump fluence, we conclude that the signal is proportional to the carrier density. Hence, the measured decay time can be attributed to the carrier lifetime. The ultrashort lifetime of several ps is consistent with the low efficiency measured, and shows potential for further improvement since such a short lifetime is likely limited by the sample quality. In fact, similar measurements performed on nanoparticle samples show carrier lifetime of about 200 ps (see theSupporting Information). To further confirm the negative sign of the differential transmission signal, we have also detected the differential reflection signal,

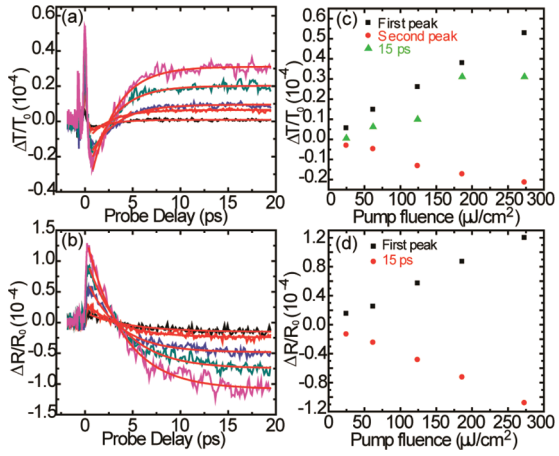

Figure 4. (a) Differential transmission and (b) reflection measured from the nanoplate thin film sample with pump fluences of (from high to low) 270, 190, 125, 60, and 25 $\mu J/cm^2$, respectively. The smooth lines are single-exponential fits with a time constant of (a) 2.4 ± 0.5 ps and (b) 3.8 ± 0.5 ps. (c, d) Signal is proportional to the pump fluence.

and found it is positive during early probe delays. Other features of the signal are similar to the differential transmission, as shown in panels b and d in Figure 4.

4. CONCLUSIONS

In summary, we have demonstrated a novel approach for the colloidal synthesis of pyrite FeS_2 nanoplates. The FeS_2 synthesis at high reaction temperature and long aging time results in the formation of hexagonal-shaped crystalline nanoplates. Although the nanoplates exhibit photovoltaic behavior with the conjugated polymer P3HT, such hybrid solar cells show the power conversion efficiency of 0.03% with an open circuit voltage of 0.78 V under AM1.5 condition. The low efficiency is likely limited by the several-ps carrier lifetime measured by an ultrafast pump−probe technique, and can be potentially improved with the sample quality. The synthesis of other doped pyrite nanoplates of general formula $M_xFe_{1-x}S_2$ (M = Zn and Li) following this synthetic protocol is under investigation (Supporting Information, Figure S2), and the results will be reported elsewhere.

■ ASSOCIATED CONTENT

Ⓢ Supporting Information

FeS_2 synthesis details, hybrid solar cell fabrication, and additional optical characterization. This material is available free of charge via the Internet at http://pubs.acs.org.

■ AUTHOR INFORMATION

Corresponding Author

*E-mail: shenqiang@ku.edu.

Notes

The authors declare no competing financial interest.

■ ACKNOWLEDGMENTS

S.R. thanks the University of Kansas for its startup financial supporting and by a subcontract from a Department of Energy award (DESC0005448). H.Z. acknowledges support from the US National Science Foundation under Awards DMR-0954486 and EPS-0903806, and matching support from the State of Kansas through Kansas Technology Enterprise Corporation.

■ REFERENCES

(1) Wadia, C.; Wu, Y.; Gul, S.; Volkman, S.; Guo, J.; Alivisatos, A. P. *Chem. Mater.* **2009**, *21*, 2568.
(2) Ennaoui, A.; Fiechter, S.; Pettenkofer, C.; Alonsovante, N.; Buker, K.; Bronold, M.; Hopfner, C.; Tributsch, H. *Sol. Energy Mater. Sol. Cells* **1993**, *29*, 289.
(3) Ennaoui, A.; Fiechter, S.; Goslowsky, H.; Tributsch, H. *J. Electrochem. Soc.* **1985**, *132*, 1579.
(4) Dasbach, R.; Willeke, G.; Blenk, O. *MRS Bull.* **1993**, *18*, 56.
(5) Wadia, C.; Alivisatos, A. P.; Kammen, D. M. *Environ. Sci. Technol.* **2009**, *43*, 2072.
(6) Steinhagen, C.; Panthani, M.; Akhavan, V.; Goodfellow, B.; Koo, B.; Korgel, B. *J. Am. Chem. Soc.* **2009**, *131*, 12554.
(7) Guo, Q.; Hillhouse, H.; Agrawal, R. *J. Am. Chem. Soc.* **2009**, *131*, 11672.
(8) Fukui, T.; Miyadai, T.; Miyahara, S. *J. Phys. Soc. Jpn.* **1971**, *31*, 1277.
(9) Hall, A. J. *Miner. Mag.* **1986**, *50*, 223.
(10) Puthussery, J.; Seefeld, S.; Berry, N.; Gibbs, M.; Law, M. *J. Am. Chem. Soc.* **2011**, *133*, 716.
(11) Disale, S.; Garje, S. *Adv. Sci. Lett* **2010**, *3*, 80.
(12) Bither, T. A.; Bouchard, R. J.; Cloud, W. H.; Donohue, P. C.; Siemons, W. J. *Inorg. Chem.* **1968**, *7*, 2208.
(13) Luck, J.; Hartmann, A.; Fiechter, S. *Anal. Chem.* **1989**, *334*, 441.
(14) Li, E. K.; Johnson, K. H.; Eastman, D. E.; Freeouf, J. L. *Phys. Rev. Lett.* **1974**, *32*, 470.
(15) Goebl, J.; Zhang, Q.; He, L.; Yin, Y. *Angew. Chem., Int. Ed.* **2012**, *51*, 552.
(16) Birkholz, M.; Fiechter, S.; Hartmann, A.; Tributsch, H. *Phys. Rev. B* **1991**, *43*, 11926.
(17) Boughriet, A.; Figueiredo, R. S.; Laureyns, J.; Recourt, P. *J. Chem. Soc., Faraday Trans.* **1997**, *93*, 3209.
(18) Azaroff, L. V. In *Elements of X-Ray Crystallography*; McGraw-Hill: New York, 1968; p 549.
(19) Lalvani, S. B.; Weston, A.; Masden, J. T. *J. Mater. Sci.* **1990**, *25*, 107.
(20) Smestad, G.; Ennaoui, A.; Fiechter, S.; Tributsch, H.; Hofmann, W. K.; Birkholz, M.; Kautek, W. *Sol. Energy Mater.* **1990**, *20*, 149.
(21) Werake, L.; Zhao, H. *Nat. Phys.* **2010**, *6*, 875.